



# Influence of electric fields on the efficiency of multilayer graphene membrane

M. Kargar<sup>1</sup> · F. Khashei Varnamkhasti<sup>1</sup> · A. Lohrasebi<sup>1,2</sup> 

Received: 23 April 2018 / Accepted: 1 August 2018 / Published online: 18 August 2018  
© Springer-Verlag GmbH Germany, part of Springer Nature 2018

## Abstract

Multilayer graphene membranes could be considered as an efficient membrane in water desalination processes based on the reverse osmosis (RO) method. In this study, we designed multilayer graphene channels using the molecular dynamics (MD) simulation approach. The effects of different parameters, such as channel width and length, and the pressure on the operation of the designed channels were examined, in the absence and presence of electric fields with various amplitudes and directions. The results indicated that the ion separation and water flow through the channels were modified under the application of the electric fields. Additionally, it has been shown that salt rejection and water flow could be controlled by the channel's structural parameters mentioned above. The obtained results of this study at the molecular level can improve the knowledge of designing membranes for water purification processes.

**Keywords** Water desalination · External electric field · Graphene channel · Molecular dynamics simulation

## Introduction

Rapid population growth raises demand for fresh water while the natural resources of fresh water are limited. Desalination of seawater and saline groundwater can be employed as the practical alternatives to overcome this challenge. Reverse osmosis (RO) desalination is one of the promising desalination methods by removing salts and dissolved mineral particles from water with the aid of pressure-driven membrane technology. Among the utilized membrane in the RO desalination, carbon-based membranes such as graphene sheets have attracted the most attention due to their advantages, such as high water permeability and high salt rejection rate [1–4].

Designing and modifying graphene-based membranes have been investigated in many computational and

experimental studies [5–8]. Using the MD simulation method, the characteristics of the graphene membrane, such as nanoporous size, density, and its functionality, have been controlled to increase their water permeability and salt rejection (two important parameters of the membrane efficiency) [9–12]. For example, hydrophilic and hydrophobic behaviors of the porous graphene have been considered, by Cohen-Tanugi et al., as a key factor to control the water flow through the graphene membrane [13]. The electrical charges of nanopores edge were used as another factor to enhance the membrane salt rejection [14]. Theoretically, water flow through a planar graphene nanochannel was planned using the channel structural parameters to create high-speed flow [15, 16]. In some relevant experimental studies, the filtration efficiency of monolayer graphene membranes was examined by considering membrane structural parameters, such as pore density and size [13, 17, 18]. Perreault et al. [19] have used multilayer graphene sheet as a highly ordered film. In some other experimental investigations, the influences of graphene sheets alignment and membrane hydrophobicity on the water permeability were measured [20–23].

Due to the polar nature of water molecules, application of a constant or alternating electric field could affect the water molecules actions. So far, some influences of external electric fields on the micro/nano-fluidic behavior of water have been considered in several studies [23–30]. It

---

**Electronic supplementary material** The online version of this article (<https://doi.org/10.1007/s00894-018-3774-9>) contains supplementary material, which is available to authorized users.

---

✉ A. Lohrasebi  
lohrasebi@nano.ipm.ac.ir

<sup>1</sup> Department of Physics, University of Isfahan, Isfahan 8174673441, Iran

<sup>2</sup> School of Nano-Science, Institute for Research in Fundamental Sciences (IPM), Tehran 193955531, Iran

has been reported that applying electric fields caused water molecules to align along the field direction, which perturbed the dynamic of water molecules, especially in the nanoscale systems. In our previous studies [8, 29], the influence of electric fields on the desalination process with the aid of multilayer nanoporous graphene membranes was investigated. In addition, the shape and motion of a water droplet on the flexible graphene sheet was considered. So it seems that investigation of the effects of electric fields on the operation of the carbon-based membranes used in the RO desalination processes could be valuable.

In the current research, a membrane made of a high-efficiency graphene-based nanochannel was designed to produce fresh water. The effects of different channel structural parameters on its operation were investigated by employing the MD simulation method. Furthermore, the influences of the application of constant electric fields on the channel efficiency were considered. The obtained results indicated the motions of water molecules and salt ions perturbed when the system was exposed to the external fields. Therefore, the application of electric fields could be used to improve the salt rejection and water flow through the channel. The results of this study may be helpful for a better understanding of the nanoscale interactions in such systems, and hence increase the knowledge of designing high-performance membranes used in water desalination processes.

## Molecular models and simulation details

Our simulation setup consisted of a multilayer graphene nanochannel, which connected the two water reservoirs on both sides of the channel (Box I and Box II). The nanochannel was made of the six-graphene parallel sheets aligned in the  $y$ -direction, with a length of  $L \in \{20, 30, \text{ and } 40 \text{ \AA}\}$  and the interlayer distance of  $h \in \{6 \text{ to } 10 \text{ \AA}\}$ , illustrated in Fig. 1. Some similar multilayer graphene-based nanochannels were experimentally used as nanochannels in filtration processes [20–23]. At the start of the simulations, box (I) was filled with saline water. The number of water molecules changed between 2190 and 3315, and the number of ions varied between 48 and 72 (depending on the  $h$  value) to make salt water with the salinity of 35 g/L. An additional graphene layer (a rigid piston) pushed the solution toward the nanochannel (the applied pressure range varied between 1 to 7 atm).

All MD simulations were performed using the Large-scale Atomic/Molecular Massively Parallel Simulator (LAMMPS) package [31], and NVT ensemble was employed. The temperature of the system was maintained at  $T = 300 \text{ K}$  using the Nose-Hoover thermostat, and the

long-range electrostatic interactions were computed with the particle-particle particle-mesh (PPPM) method. The intermolecular interactions between the carbon atoms in the graphene sheets were calculated with the adaptive intermolecular reactive empirical bond order (AIREBO) potential. The transferable intermolecular potential 4 points (TIP4P) model was employed to model the water molecules interactions. Moreover, the extended single point charge (SPC/E) water model was used. The Lennard-Jones (LJ) potential described the nonbonding interactions between particles and the related parameters are listed in Table 1 [32], and the Lorentz-Berthelot mixing rule was used for cross interactions. A cutoff radius of 10 Å and 8.5 Å were used to compute the van der Waals and the Columbic interactions, respectively. The equations of motion were integrated via the velocity verlet method, with the time-step of 1 fs, and the periodic boundary conditions were imposed in all directions.

In all simulations, at first, the system was equilibrated during 100 ps of simulation time, in which the velocity of the rigid piston was kept at zero, and the water molecules and the ions were not allowed to enter the channel. During the equilibrium, the energy of the system was examined to make sure the system had reached the equilibration. Following this phase, several simulations of the period of 3 ns were carried out, to study the impacts of some channel structural parameters, such as layer separation distance and channels thickness on the nanochannel performance. To investigate the influence of electric field orientation and amplitude, the system was simulated in the presence of the electric fields in the  $Y$ - and  $Z$ -directions with the amplitude of  $E = 0, 0.04, 0.08, 0.12, \text{ and } 0.16 \text{ V/\AA}$ . In addition, the effect of the flexibility of the channel walls on the membrane performance was studied by considering two conditions; case (1) all atoms of graphene sheets were fixed, case (2) some atoms of graphene sheets in the internal and external parts of the channel were fixed (atoms in sections A and B were fixed as shown in Fig. 1a).

## Results and discussion

As mentioned above, the saline water filtration using the multilayer graphene nanochannel, with different structural parameters, was investigated by performing MD simulations. We explain the process for a typical case to obtain a better understanding of the nanochannel operation:

By applying a pressure to the rigid piston along the  $y$ -direction, the NaCl-solution pushed toward the channel. The water molecules passed through the channel and entered box II, while most of the positive and negative ions within box I could not enter the channel, because their

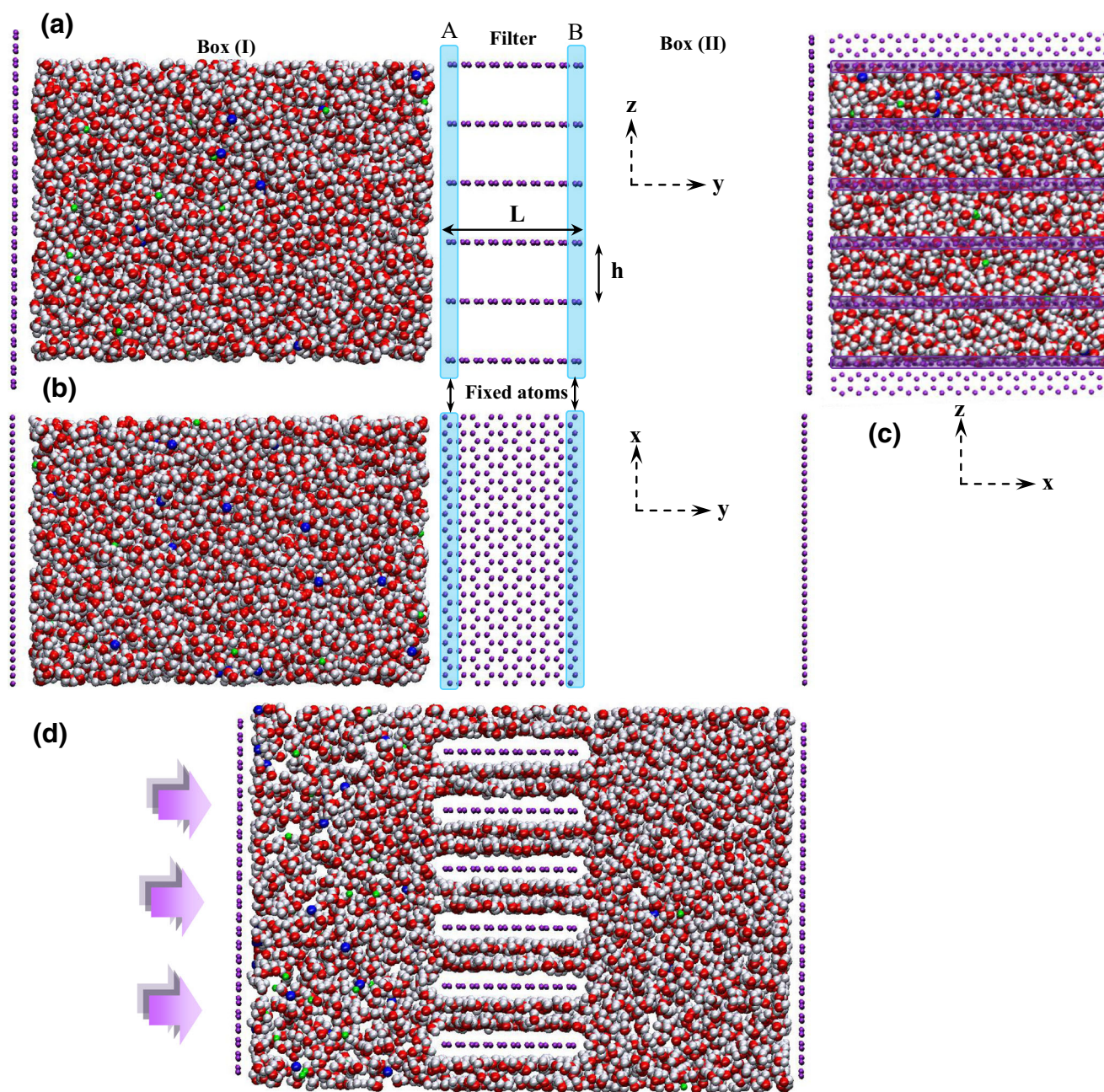


**Fig. 1** The structure of the designed system components: (a) side view; (b) top view; (c) front view. The nanofilter is composed of multilayer graphene sheets, which connected the two water reservoirs

**Table 1** Lennard-Jones parameters used in this study

Type	Atom	$\sigma$ (nm)	$\epsilon$ (kcal mol <sup>-1</sup> )	q (e)
Water	O	0.31589	0.1852	-0.834
Water	H	0.0	0.0	+0.417
Graphene	C	0.12	3.214	0.0
Ions	Na	0.22589	0.1684	+1.0
	Cl	0.51645	0.117	-1.0

hydration radii were usually bigger than the channel inter-layer separation (The radii of the hydrated Na<sup>+</sup> and Cl<sup>-</sup> are about 3.6 and 3.3 Å, respectively [33]). Therefore, only dehydrated ions could enter the channel, and since the reservoir could rarely supply the dehydration energy, only a few of these ions can pass through the channel. Hence, the less thick the channels, the less likely the ion passes and the higher percentage of salt rejection will be achieved. On the other hand, decreasing the channel thickness led to reducing the water flow through the channel (movie 1.avi

shows the dynamic of the saline water through the multi-layer membrane).

The ion rejection values ( $\frac{\text{number of ions} - \text{number of passed ions}}{\text{number of ions}} \times 100$ ) and water flow rate (linear slope of the number of passed water molecules through the channel as a function of the simulation time) for cases 1 and 2 with different inter-layering distances are shown in Fig. 2a. As was expected, increasing the interlayer distances enhanced the water flow rate, while it decreased the ion rejection, especially in case 2 (the flexible channels). It might be due to the movement of unfixed carbon atoms of the channel, which perturb the dynamics of the ions and the water molecules inside the channels. This perturbation may lead to increased passage of ions through the membrane. Moreover, the water molecules compression inside the channels was calculated in the steady-state condition (the situation that the water flow rate through the channel was nearly constant). The obtained results for both cases, with different interlayer distances, are presented in Fig. 2b. It can be seen that the minimum water molecules compression was obtained at the interlayer distance of 8 Å, which was due to the water molecules arrangement inside the channel. At the interlayer distance of 7 Å, the water molecules shaped a one-layer structure

during their transport across the channel, and at the inter-layer distance of 9 Å, they shaped a two-layer structure. So, at  $h = 8$  Å, the accessible channel interlayer space for water molecules was more than the space to form the one-layer and less than to shape the two-layer structure of the water molecules. Therefore, at  $h = 8$  Å the water molecules flowed between the graphene layers with the lower compression, in comparison with the interlayer distances of  $h = 7$  and 9 Å. The schematic view of water flow through the channels with different interlayer distances (at the steady-state condition) and their corresponding water molecular distribution profiles among the channels are shown in panels of Fig. 3. The observed peaks in the distribution profile correspond to the positions with the most water molecules and imply that the water molecules inside the channels formed layer structures during their transition across the channels. It can be seen that at  $h = 6$  and 7 Å, the one-layer configuration was shaped, and at  $h = 9$  and 10 Å, the two-layer pattern was formed, while at the channel width of 8 Å, water molecules flowed through the channels in a special arrangement thicker than the one-layer structure. Three channels of the lengths 20, 30, and 40 Å were examined, with the interlayer distance of 10 Å, to consider the effect of the channel's length on the membrane operation. The results reported in Table 2 indicate that the water flow decreases by increasing the channel length, while the ion rejection percent increases.

It should be noticed that, an external electric field was exposed to the system to evaluate the effects of the electric field on the operation of the membrane, and the field amplitude and direction were changed in the different simulations ( $E = 0, 0.04, 0.08, 0.12,$  and  $0.16$  V/Å in the  $z$  and  $y$  directions). Application of the electric field could effect both the motions of ions and water molecules in the system, which can perturb the general performance of the channel (a movie entitled "Mov 1.avi" is provided to show the dynamics of the system with  $h = 7$  Å and under the application of the electric field of  $0.12$  V/Å). At first, the  $z$ -direction electric field was applied on the channel of width  $h = 10$  Å for case 1, in which all carbon atoms of the channel were fixed during the simulation. Figure 4 shows the water flow and salt rejection percentage as a function of amplitude of the applied  $z$ -direction electric field. It was observed that the channel performance enhanced when the amplitude of the electric field was increased, i.e., the water flow and salt rejection percentage were increased. The diffusion coefficient of the water molecule,  $D$ , in the channel was calculated (by using the velocity of the water molecules) in the absence and presence of the electric field, for different channel widths. The presented results in Fig. 5 show the ratios of  $D/D_0$  for the different channels, in which  $D_0$  is the diffusion coefficient of the water molecule in the channel with  $h = 6$  Å. It was

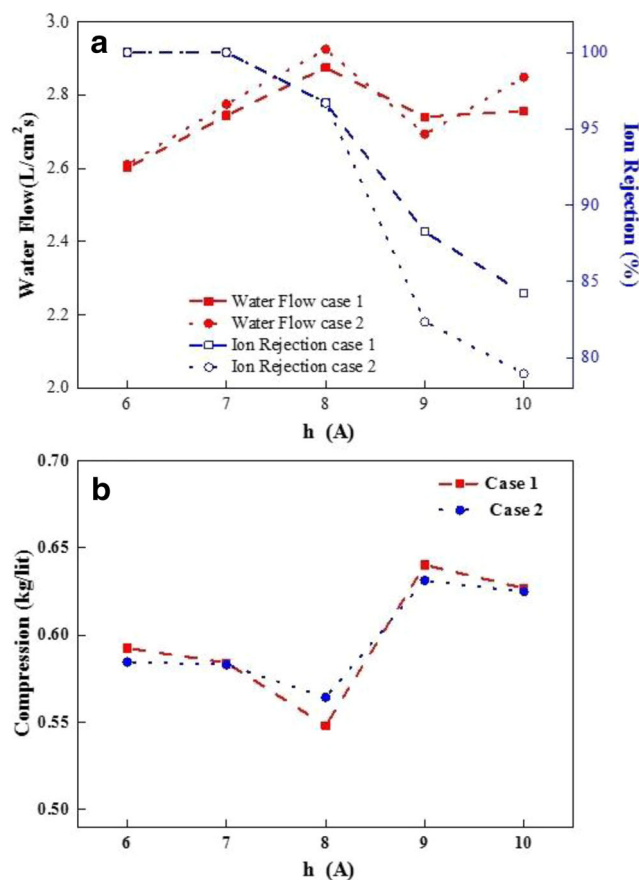


**Fig. 2** (a) The water flow rate, and (b) the ion rejection values for the cases 1 and 2 with different inter-layering distances

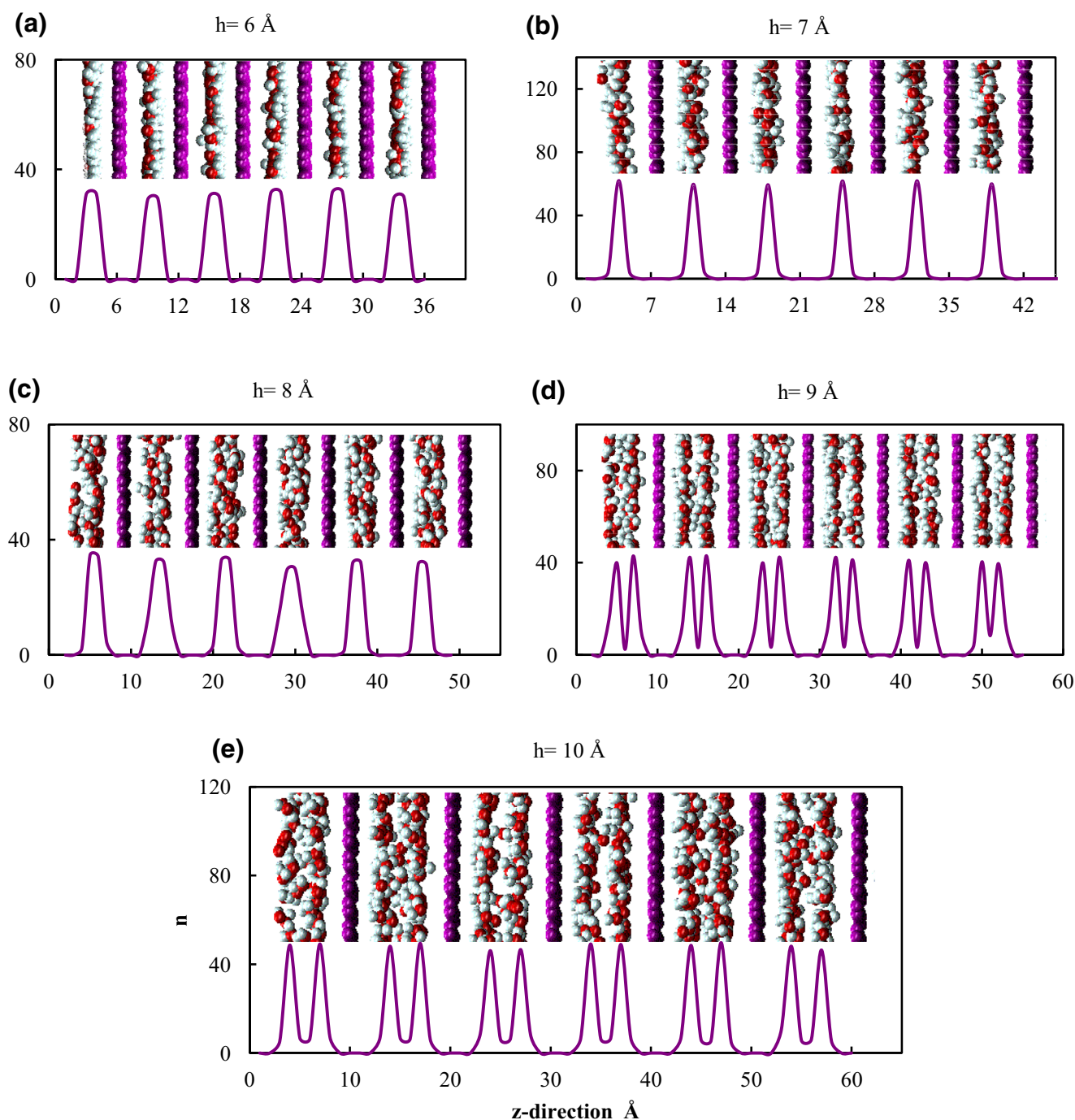


**Fig. 3** The schematic view of water flow through the channels for different channels and their corresponding water molecular distribution profiles

**Table 2** The average percentage of rejected ions and water flow through the multilayer graphene membrane of the lengths of 20, 30, and 40 Å, with interlayer separation of 10 Å and applied pressure of 1.7 atm

Multilayer graphene membrane for NaCl solution			
	L = 20 Å	L = 30 Å	L = 40 Å
Ion rejection percentage	83.7	87.4	92.2
Water flow (L/cm <sup>2</sup> s)	2.69	2.57	2.49

found that this value,  $D/D_0$ , was increased by enlarging the channel, and was reduced under the application of the electric field. Moreover, it was seen that when the electric field was applied, the water molecules generally aligned along the field. The obtained results of the simulations showed that the average alignment of water molecules in the three division of the system, i.e., box (I), filter, and box (II), were not similar in the presence of the external electric field. It was found that the average angles between the

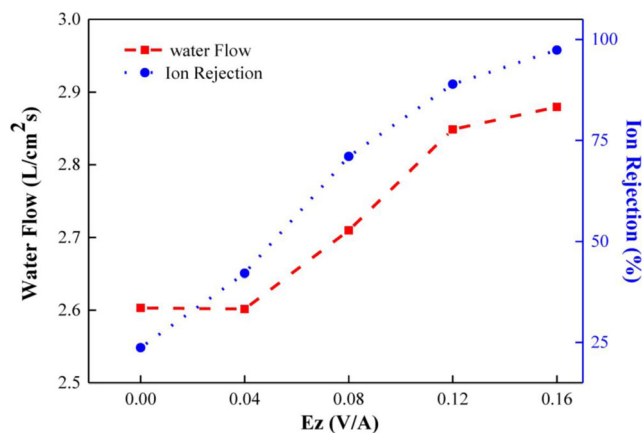


**Fig. 4** Water flow and salt rejection percentage when the electric field is applied in the z-direction on the channel of width  $h = 10 \text{ \AA}$

water dipoles and the applied field,  $\theta$ , were decreased whenever the water molecules passed the channel's ends, i.e., once they entered the channel from the first box and during the exiting from the channel to the second box. The average of  $\cos(\theta)$  for various channels under the application of the electric field of  $0.12 \text{ V/\AA}$  are listed in Table 3. As can be seen, the maximum values of  $\cos(\theta)$  were observed in the first box, and the minimum values were obtained in the second box. The variation of water molecules orientation when the system was exposed to the electric field of  $0.12 \text{ V/\AA}$  is shown in Fig. 6, for the channel widths of 6 and  $10 \text{ \AA}$ .

Then the electric fields with different amplitudes were applied in the y-direction. It was seen that during the simulation, positive and negative ions separated from each other, i.e., positive ions entered the second box while the negative ions remained in the first box. The negative ions in the first box experienced the additional force from the applied field

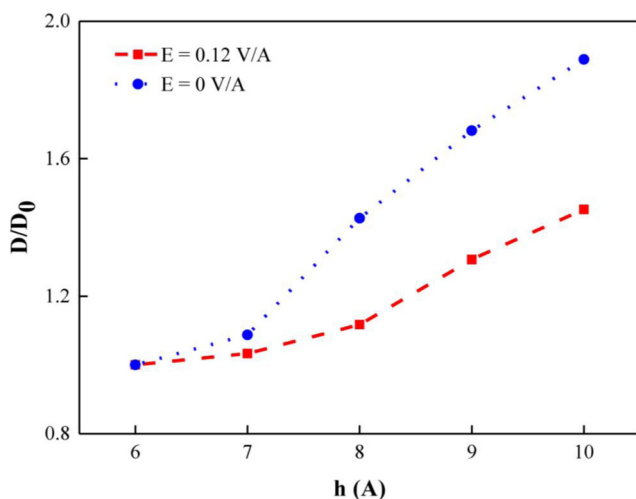


**Fig. 5** The ratios of the diffusion coefficient of the water molecule for the different channels ( $D$ ) and the diffusion coefficient of the water molecule in the channel with  $h = 6 \text{ \AA}$  ( $D_0$ ), as a function of applied electric fields

**Table 3** The average of  $\cos(\theta)$  for various channels under the application of the electric field of  $0.12 \text{ V/\AA}$

The average of  $\cos(\theta)$  for the water dipoles and the applied field

Channel width (Å)	Box(I)	Filter	Box(II)
10	0.71922	0.64186	0.56209
9	0.71699	0.62402	0.59214
8	0.71699	0.62402	0.59214
7	0.71699	0.62402	0.59214
6	0.72209	0.54699	0.55225

that pushed them toward the piston and caused them to apply an extra force on the piston. Therefore, more pressure must be exerted on the piston to push the water toward the channel. Figure 7 shows the water flow and the applied pressure on the piston as a function of amplitude of the applied y-direction electric field. Curves of Fig. 7 show the variation of the water flow through the channel versus

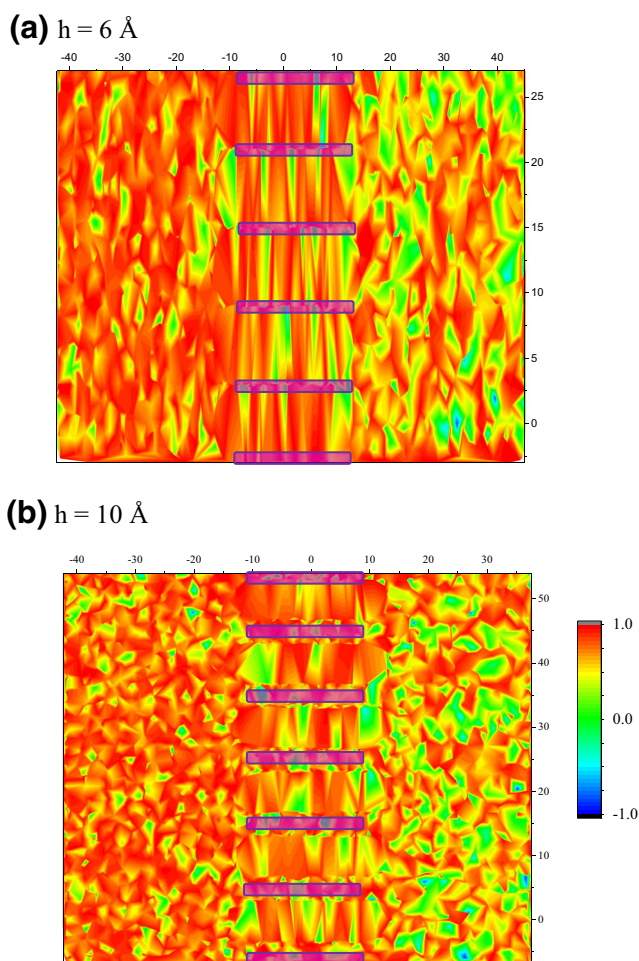


**Fig. 6** Variation of water molecules orientation,  $\cos(\theta)$ , when the system was exposed to the electric field of  $0.12 \text{ V/\AA}$ , for the channel widths of  $6 \text{ \AA}$  (a) and  $10 \text{ \AA}$  (b)

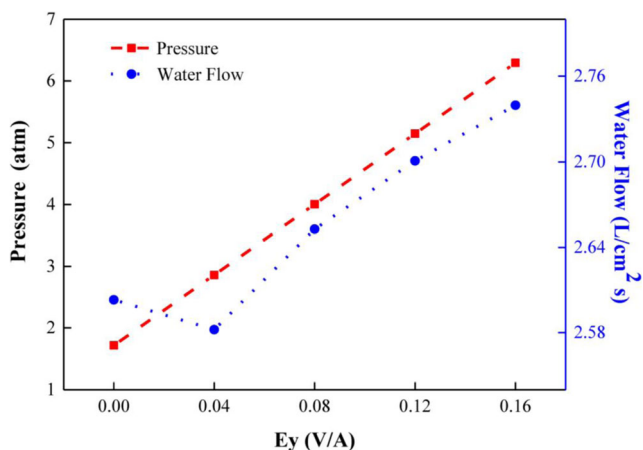


**Fig. 7** Variation of the water flow through the channel with  $h = 10 \text{ \AA}$  versus the needed pressure corresponding to the applied fields

the applied pressure, for the different fields and channel width of  $h = 10 \text{ \AA}$ . It can be seen that by increasing the applied field, more pressure was required to create the nearly fixed water flow rate across the channels. For example, when the electric field of  $0.08 \text{ V/\AA}$  was exposed to the system, a pressure of 4 atm needed to be applied to the piston, while exposing the field of  $0.16 \text{ V/\AA}$  caused the pressure to increase to about 6.29 atm, to create the same water flow rate through the channels.

To examine the effect of channel thickness on the dynamics of particles, in the absence and presence of the electric fields, we calculated the average deceleration of water molecules. For this purpose, during the steady-state condition the applied pressure was removed, reducing the average velocity of water molecules inside the channel. The computed average decelerations of water molecules are shown in Fig. 8 for different channel thicknesses in the absence and presence of  $E = 0.12 \text{ V/\AA}$ . As can be seen, exposing the channel to the electric field caused the average deceleration of water molecules to increase, which could be due to the water molecules response to the applied field.

Finally, some more simulations were conducted to consider the performance of the channel for KCl,  $\text{CaCl}_2$ ,  $\text{MgCl}_2$ , and  $\text{FeCl}_3$  solutions. The very similar results of NaCl solution were obtained, which are presented in Table 4. It was found that the membrane separated the positive ions ( $\text{K}/\text{Ca}^{2+}/\text{Mg}^{2+}/\text{Fe}^{3+}$ ) and negative ions ( $\text{Cl}^-$ ) from each other, with nearly the same water flow rate of NaCl solution.

**Table 4** Ion separation percentage for KCl,  $\text{CaCl}_2$ ,  $\text{MgCl}_2$ , and  $\text{FeCl}_3$  solution and water flow percentage for NaCl solution under an applied pressure of 2 atm

$L = 20 \text{ \AA}$ , $h = 10 \text{ \AA}$ , $E = 0.12 \text{ V/\AA}$	KCl	$\text{MgCl}_2$	$\text{CaCl}_2$	$\text{FeCl}_3$
Ion rejection percentage	94.74	94.74	94.74	97.37
Water flow ( $\text{L}/\text{cm}^2\text{s}$ )	3.70	3.93	3.61	3.57

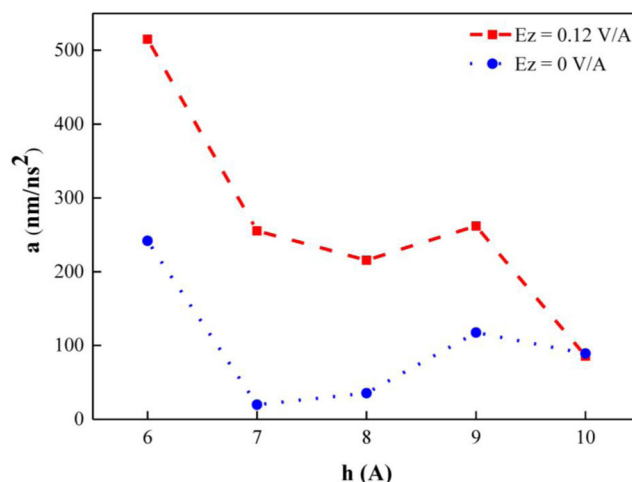


**Fig. 8** Average of water molecules deceleration as a function of channel thicknesses in the absence and presence of  $E = 0.12 \text{ V/\AA}$

### Conclusions

In this study, we considered the influences of some structural and environmental parameters on the operation of the multilayer graphene channels, which can be used in water purification processes. For this purpose, the deterministic MD simulation method was employed to model the dynamics of the system and examine the influence of the interlayer separation distance and application of external electric fields on the channel efficiency.

We found that, as far as the interlayer separation distance was concerned, the water flow through the channel was increased by enhancing the separation distance, while the ion rejection percentage was reduced. Also, it was shown that the water flow and ion rejection percentage depend on the channel thickness. We also observed that exposing the system to the suitable external electric field can lead to an improvement in the water flow and ion rejection by influencing the arrangement of water molecules in the channel. Furthermore, our simulation results indicated that we could use the axial electric fields to separate positive and negative ions, increasing the needed applied pressure on the system.

### References

- Konatham D, Yu J, Ho TA, Striolo A (2013) Simulation insights for graphene-based water desalination membranes. *Langmuir* 29: 11884–11897
- Cohen-Tanugi D, McGovern RK, Dave SH, Lienhard JH, Grossman JC (2014) Quantifying the potential of ultra-permeable membranes for water desalination. *Energy Environ Sci* 7:1134–1141
- Rikhtehgaran S, Lohrasebi A (2015) Water desalination by a designed nanofilter of graphene-charged carbon nanotube: a molecular dynamics study. *Desalination* 365:176–181

4. Homaeigohar S, Elbahri M (2017) Graphene membranes for water desalination. *NPG Asia Mater* 9:e427. <https://doi.org/10.1038/am.2017.135>
5. Cohen-Tanugi D, Grossman JC (2012) Water desalination across nanoporous graphene. *Nano Lett* 12:3602–3608
6. Sun P, Wang K, Zhu H (2016) Recent developments in graphene-based membranes: structure, mass-transport mechanism and potential applications. *Adv Mater* 28:2287–2310
7. Abraham J, Vasu KS, Williams CD, Gopinadhan K, Su Y, Cherian CT, Dix J, Prestat E, Haigh SJ, Grigorieva IV (2017) Tunable sieving of ions using graphene oxide membranes. *Nat Nanotechnol* 12: 546–550
8. Lohrasebi A, Rikhtehgaran S (2018) Ion separation and water purification by applying external electric field on porous graphene membrane. *Nano Res* 11(4):2229–2236
9. Wang EN, Karnik R (2012) Water desalination: graphene cleans up water. *Nat Nanotechnol* 7:552
10. O'Hern SC, Stewart CA, Boutilier MS, Idrobo JC, Bhaviripudi S, Das SK, Kong J, Laoui T, Atieh M, Karnik R (2012) Selective molecular transport through intrinsic defects in a single layer of CVD graphene. *ACS Nano* 6:10130–10138
11. Nicolai A, Sumpter BG, Meunier V (2014) Tunable water desalination across graphene oxide framework membranes. *Phys Chem Chem Phys* 16:8646–8654
12. An D, Yang L, Wang TJ, Liu B (2016) Separation performance of graphene oxide membrane in aqueous solution. *Ind Eng Chem Res* 55:4803–4810
13. Cohen-Tanugi D, Lin LC, Grossman JC (2016) Multilayer nanoporous graphene membranes for water desalination. *Nano Lett* 16:1027–1033
14. Cohen-Tanugi D, Grossman JC (2015) Nanoporous graphene as a reverse osmosis membrane: recent insights from theory and simulation. *Desalination* 366:59–70
15. Kumar Kannam S, Todd B, Hansen JS, Daivis PJ (2012) Slip length of water on graphene: limitations of non-equilibrium molecular dynamics simulations. *J Chem Phys* 136:024705
16. Dahanayaka M, Liu B, Hu Z, Pei QX, Chen Z, Law AWK, Zhou K (2017) Graphene membranes with nanoslits for seawater desalination via forward osmosis. *Phys Chem Chem Phys* 19:30551–30561
17. Wu S, Yang R, Shi D, Zhang G (2012) Identification of structural defects in graphitic materials by gas-phase anisotropic etching. *Nanoscale* 4:2005–2009
18. O'Hern SC, Jang D, Bose S, Idrobo JC, Song Y, Laoui T, Kong J, Karnik R (2015) Nanofiltration across defect-sealed nanoporous monolayer graphene. *Nano Lett* 15:3254–3260
19. Perreault F, De Faria AF, Elimelech M (2015) Environmental applications of graphene-based nanomaterials. *Chem Soc Rev* 44: 5861–5896
20. Wang J, Zhang P, Liang B, Liu Y, Xu T, Wang L, Cao B, Pan K (2016) Graphene oxide as an effective barrier on a porous nanofibrous membrane for water treatment. *ACS Appl Mater Interfaces* 8:6211–6218
21. Cheng C, Jiang G, Garvey CJ, Wang Y, Simon GP, Liu JZ, Li D (2016) Ion transport in complex layered graphene-based membranes with tuneable interlayer spacing. *Sci Adv* 2:e1501272
22. Hong S, Constans C, Surmani Martins MV, Seow YC, Guevara Carrió JA, Garaj S (2017) Scalable graphene-based membranes for ionic sieving with ultrahigh charge selectivity. *Nano Lett* 17: 728–732
23. Chen L, Shi G, Shen J, Peng B, Zhang B, Wang Y, Bian F, Wang J, Li D, Qian Z (2017) Ion sieving in graphene oxide membranes via cationic control of interlayer spacing. *Nature* 550:380
24. Bateni A, Susnar S, Amirfazli A, Neumann A (2004) Development of a new methodology to study drop shape and surface tension in electric fields. *Langmuir* 20:7589–7597
25. Sint K, Wang B, Král P (2008) Selective ion passage through functionalized graphene nanopores. *J Am Chem Soc* 130:16448–16449
26. Liu J, Wang M, Chen S, Robbins MO (2012) Uncovering molecular mechanisms of electrowetting and saturation with simulations. *Phys Rev Lett* 108:216101
27. Song F, Li B, Liu C (2013) Molecular dynamics simulation of nanosized water droplet spreading in an electric field. *Langmuir* 29:4266–4274
28. Corson LT, Tsakonas C, Duffy BR, Mottram NJ, Sage IC, Brown CV, Wilson SK (2014) Deformation of a nearly hemispherical conducting drop due to an electric field: theory and experiment. *Phys Fluids* 26:122106
29. Zhu J, Lan Y, Du H, Zhang Y, Su J (2016) Tuning water transport through nanochannels by changing the direction of an external electric field. *Phys Chem Chem Phys* 18:17991–17996
30. Kargar M, Lohrasebi A (2017) Deformation of water nano-droplets on graphene under the influence of constant and alternative electric fields. *Phys Chem Chem Phys* 19:26833–26838
31. Plimpton S (1995) Fast parallel algorithms for short-range molecular dynamics. *J Comput Phys* 117:1–19
32. Allen M, Tildesley DJ (1987) *Computer simulation of liquids*. Oxford University Press, New York
33. Conway BE (1981) *Ionic hydration in chemistry and biophysics*. Elsevier, New York